Osteoarthritis and Cartilage (2008) **16,** 1018–1023

doi:10.1016/j.joca.2008.01.007

Osteoarthritis and Cartilage

International Cartilage Repair Society

OARSI OSTEOARTHRITIS RESEARCH SOCIETY INTERNATIONAL

Lower cervical spine facet cartilage thickness mapping

W. Womack B.S., D. Woldtvedt and C. M. Puttlitz Ph.D., Co-Director, Assistant Professor*

Orthopaedic Bioengineering Research Laboratory, Department of Mechanical Engineering, Colorado State University, Fort Collins, CO, United States

Summary

Objective: Finite element (FE) models of the cervical spine have been used with increasing geometric fidelity to predict load transfer and range of motion (ROM) for normal, injured, and treated spines. However, FE modelers frequently treat the facet cartilage as a simple slab of constant thickness, impeding the accuracy of FE analyzes of spine kinematics and kinetics. Accurate prediction of facet joint contact forces and stresses, ROM, load transfer, and the effects of facet arthrosis require accurate representation of the geometry of the articular cartilage of the posterior facets. Previous research has described the orientations of the facet surfaces, their size and aspect ratio, and mean and maximum thickness. However, the perimeter shape of the cartilaginous region and the three-dimensional distribution of cartilage thickness remain ill-defined. As such, it was the intent of this research to further quantify these parameters.

Method: Vertebrae from seven fresh-frozen unembalmed human cadavers were serially sectioned and the osteochondral interface and the articulating surface of each facet on each slice were identified. The cartilage thickness was recorded at nine equidistant points along the length of each facet. It was observed that facets tended to have elliptic or ovoid shapes, and best-fit ovoid perimeter shapes were calculated for each facet. The thickness distribution data were used to represent the entire three-dimensional cartilage distribution as a function of one variable, and a thickness distribution function was optimized to fit the thickness distribution. The antero-posterior and medial/lateral shifts of the thickness center relative to the geometric were calculated and reported.

Results: High correlation was observed between the ovoid perimeter shapes and the measured facet shapes in radial coordinates, indicating that the ovoid approximation is able to accurately represent the range of facet geometries observed. High correlation between the measured and fitted thickness distributions indicates that the fitting function used is able to accurately represent the range of cartilage thickness distributions observed.

Conclusion: Utilization of a more physiologic cartilage thickness distribution in FE models will result in improved representation of cervical spine kinematics and increased predictive power. The consistency observed in the thickness distribution function in this study indicates that such a representation can be generated relatively easily.

Key words: Cartilage, Thickness mapping, Cervical spine, Facet joints.

Introduction

Spinal degenerative disorders affect many people annually in the United States alone, and substantial research efforts have been expended with regard to the treatment of these disorders[1]. The posterior facet joints have been shown to play a major role in spinal diseases via cartilage degeneration, arthrosis, and traumatic failure[2]. Computational finite element (FE) models of the cervical spine have been used with increasing geometric fidelity to predict spinal load transfer and range of motion (ROM) in the normal, injured, and treated conditions. However, while the osseous geometry is easily reconstructed using quantitative Computed Tomography (qCT) data, the associated soft tissue reconstructions cannot be accomplished with reasonable fidelity using this radiographic approach[3]. As a result, FE modelers frequently simplify the facet cartilage as a simple homogenous block of constant thickness extruded from the underlying bone, which may be further simplified as a planar surface. Our preliminary data (unpublished) indicate that this modeling technique reduces the accuracy of FE analyses with respect to spine kinematics/kinetics and the predictions of internal mechanical parameters such as contact pressure, stress, strain, etc. Accurate predictions of facet joint contact forces and stresses, ROM, load transfer, and the effects of facet arthrosis require an accurate anatomic representation of the posterior facet articular cartilage geometry.

Previous research has described the orientations of the facet surfaces, their size and aspect ratio, and mean and maximum cartilage[4–6]. The antero-posterior (AP) width and thickness profiles of the facet cartilage on the mid-sagittal plane have been described as well[6]. However, a mathematical description of the entire perimeter shape of the cartilaginous region and a fully three-dimensional mapping of cartilage thickness across the entire facet surface has not been reported. Therefore, the purpose of this study was to obtain a sample of facet cartilage distributions, and from this data, provide a statistical description of the aforementioned parameters across the sample population.

*Address correspondence and reprint requests to: Dr Christian M. Puttlitz, Ph.D., Co-Director, Assistant Professor, Orthopaedic Bioengineering Research Laboratory, Department of Mechanical Engineering, 1374 Campus Delivery, Colorado State University, Fort Collins, CO 80523-1374, United States. Tel: 1 970 491 0956 (Engineering Office); Fax: 1 970 297 4150; E-mail: puttlitz@engr.colostate.edu

Received 5 September 2007; revision accepted 14 January 2008.

Methods

Vertebrae from seven fresh-frozen, unembalmed, human cadaver cervical (C3–C7) vertebral columns (mean age 42: 33–50 yrs) were used in this study. Soft tissues were removed and the individual vertebrae were isolated by resection of the intervertebral discs and synovial joints, with particular care taken not to disrupt the cartilaginous surfaces of the facets. Full hydration was maintained throughout the experiment with isotonic saline solution (8.5 g/L of ACS grade Sodium Chloride, VWR International, Westchester, PA). Each vertebra was serially sectioned in the sagittal plane from laterally to medially in 1.0 mm increments using a diamond-bladed band saw (Model 3031 CP/N, Exakt Technologies, Oklahoma City, OK) across the entire facet. Both the left and right superior and inferior articular facets were sectioned in this manner. A total of 25 vertebrae from the C3 to C7 levels were used. Levels that were observed to be damaged or degenerated were excluded.

Each slice was immediately dyed with a 1% Toluidine Blue solution (Fisher Scientific, Fair Lawn, NJ) to delineate the osteochondral boundaries of the articular cartilage. Individual slices were digitally photographed at 42 micron pixel resolution (5 Megapixel digital camera, Canon USA, Lake Success, NY) along with an accompanying scale and appropriate labels were incorporated in the images representing the source (specimen and level) and medial/lateral (ML) position of the slice so that three-dimensional reconstructions of facet geometry could be performed (Fig. 1). Consistent orientation was maintained between slices.

A custom-written image analysis algorithm, coded in Visual Basic (Microsoft Corp., Redmond, WA) traced the osteochondral interface and the articulating surface of each facet parametrically (Fig. 2). The anterior and posterior endpoints of each cartilage section were manually delineated, and the cartilage thickness was calculated and recorded at nine equidistant points along the length. The positions of the osteochondral interface and the articulating surface relative to a perpendicular bisecting line connecting the endpoints were recorded in order to describe the AP curvatures of both surfaces. This procedure was performed for each image of each facet (a total of 887 images).

The AP widths of the cartilage in each slice were registered and aligned to map the shape of the perimeter of each facet. It was observed that facets tended to have elliptic or ovoid shapes. Therefore, best-fit ovoid perimeter shapes were calculated for each facet consisting of two hemi-ellipses with identical AP widths. The ML and AP widths of each facet were recorded, as well as the ML shift (δ_L) of the ovoid centerline (defined as the ML position that corresponded to the maximum AP width) relative to the geometric center (mid-span) (Fig. 3). The medial and lateral endpoints could not be precisely identified because the facets were sectioned sagittally, resulting in a 1.0 mm resolution for detecting the ML boundaries. The best-fit boundaries were approximated by extrapolating the perimeter profile and mean thickness profile.

The best-fit perimeter for each facet provided the basis for a modified cylindrical coordinate system, located at approximately the location of maximum thickness. The thickness data were mapped from the three-dimensional point cloud (x,y,t, where t is thickness) to cylindrical coordinates (r,θ,t). A transformed radius function (r_{ratio}) was then utilized:

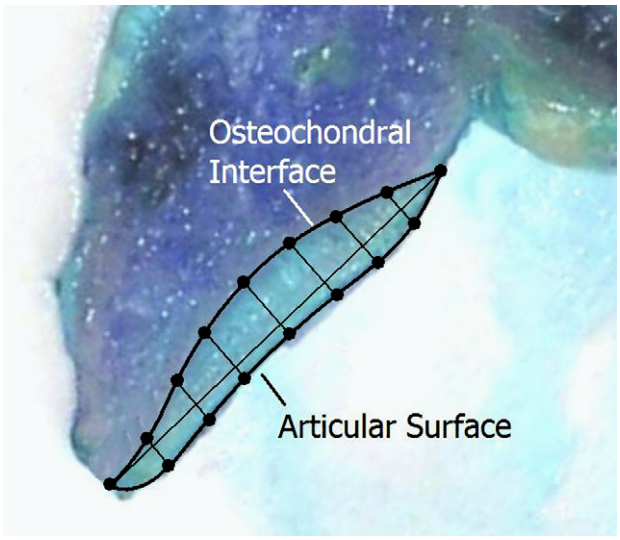

Fig. 2. Mapping of osteochondral interface and facet surface.

$$r_{ratio}(r,\theta) = \frac{r}{r_{perim}(\theta)} \quad (1)$$

where r_{perim} is the radius of the facet perimeter at orientation θ, such that $r_{ratio} = 0$ at the coordinate reference position (where thickness is maximized), and $r_{ratio} = 1$ along the perimeter. Using this technique it was possible to represent the entire three-dimensional cartilage distribution as a function of one variable (r_{ratio}). A thickness distribution function, $t_{fit}(r_{ratio})$, was optimized to fit the thickness distribution data:

$$t_{fit}(r_{ratio}) = t_{max}\left[\cos\left(\frac{\pi r_{ratio}}{2}\right)\right]^k \quad (2)$$

The parameters t_{max} and k, the maximum thickness and shape parameter respectively, were found independently for each facet. Cartilage thickness distributions and shape parameters for each facet were found by iteratively minimizing the difference between the measured and idealized thickness distributions by simultaneously varying t_{max}, k, and the AP and ML positions of the modified cylindrical coordinate reference frame (defined as the location of maximum thickness of the idealized thickness distribution). This

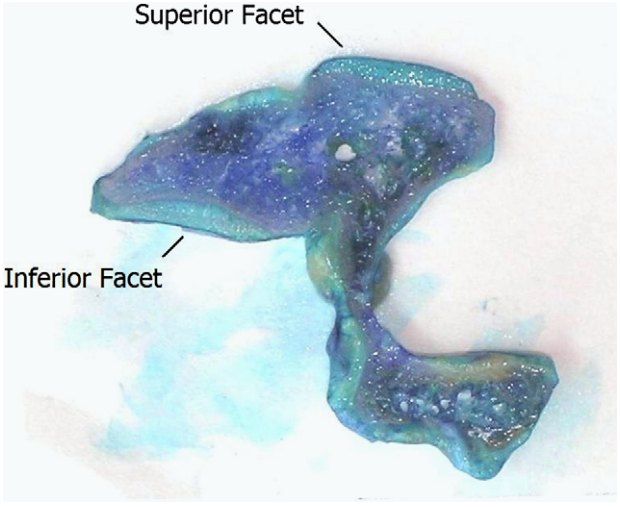

Fig. 1. Facets were serially sectioned, dyed with 1% Toluidine Blue solution, and digitally photographed.

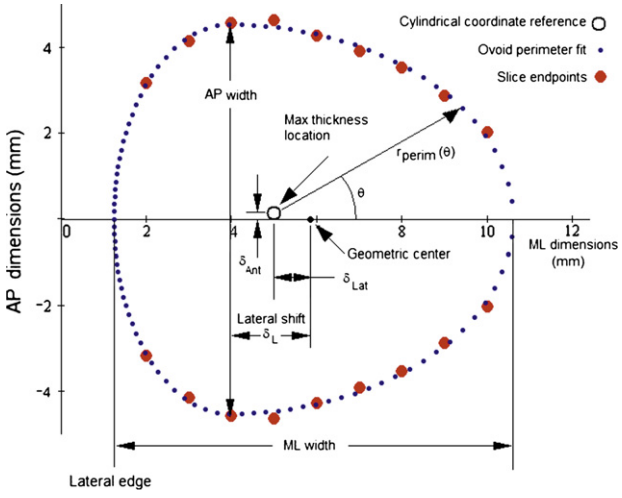

Fig. 3. Ovoid perimeter fit for a representative facet. Geometric center, ovoid centerline, and location of maximum thickness (cylindrical coordinate reference) noted.

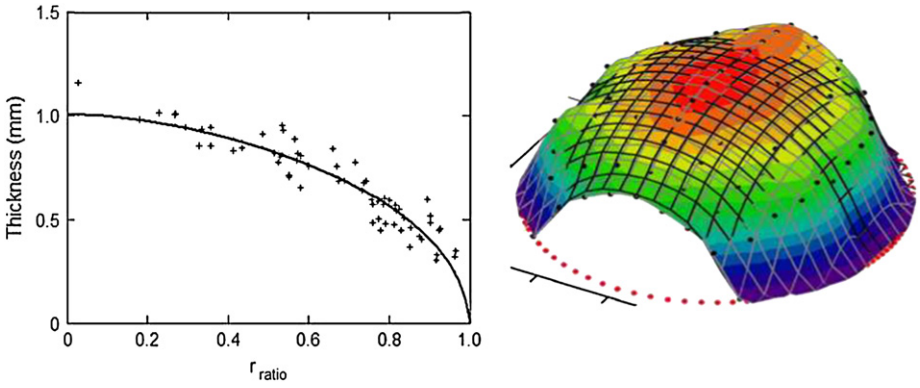

Fig. 4. Cartilage thickness distribution and fit for a representative facet, where $t_{max} = 1.00$ mm and $k = 0.48$, as a function of r_{ratio} (left) and mapped in three dimensions (right, thickness scale magnified). Color surface and dots represent measured data and the black grid represents the analytical thickness fitting function.

computational approach provided for a robust fitting function of relatively few parameters that capably represented a wide variety of perimeter shapes and thickness distributions (Fig. 4). The AP and ML shifts of the thickness center relative to the geometric center and ovoid centerline were calculated and reported (Fig. 3). Statistical significance in the aforementioned parameters was determined using paired *t*-tests between inferior and superior facets and unpaired *t*-tests between levels, where *P*-values less than 0.05 were considered statistically significant. Differences between inferior and superior facets as well as differences by vertebral level were examined. Pearson's correlation coefficients were calculated between measured and ovoid fit perimeter shapes in radial coordinates, as well as between fitted and measured thickness distributions.

Results

High correlation (mean $r^2 = 0.96$) was observed between the ovoid perimeter shapes and the measured facet shapes in radial coordinates (indicating that the ovoid approximation accurately represents the range of facet perimeter geometries observed) (Fig. 3). No significant differences in ML facet width were found between the inferior and superior facets, but the inferior facets were found to be slightly wider in the AP direction than their superior counterparts

Table I
Summary of collected data (means with standard deviation)

Level		Facet boundary shape				Thickness distribution			Thickness shift			
		AP width (mm)	ML width (mm)	Lateral shift δ_L (mm)	Lateral shift δ_L (%)	t_{max} (mm)	t_{mean} (mm)	k	δ_{Lat} (%)	δ_{Lat} (mm)	δ_{Ant} (%)	δ_{Ant} (mm)
Superior	C3	9.13 (1.61)	10.74 (2.26)	0.75 (1.65)	6.2 (15.3)	1.14 (0.42)	0.61 (0.22)	0.48 (0.12)	3.7 (13.8)	0.38 (1.38)	0.8 (4.5)	0.04 (0.56)
	C4	8.64 (0.84)	11.54 (2.88)	0.57 (1.51)	5.9 (14.8)	1.13 (0.24)	0.57 (0.12)	0.58 (0.10)	3.5 (17.4)	0.62 (1.71)	0.4 (3.0)	0.03 (0.32)
	C5	8.94 (0.73)	12.67 (2.40)	1.03 (1.18)	8.6 (10.0)	1.04 (0.20)	0.55 (0.10)	0.53 (0.12)	4.9 (18.1)	0.78 (2.30)	−0.8 (5.0)	−0.09 (0.57)
	C6	8.95 (0.76)	12.15 (1.43)	1.60 (0.88)	13.3 (7.6)	0.97 (0.16)	0.52 (0.08)	0.44 (0.10)	−10.8 (9.9)	−1.30 (1.30)	1.4 (6.5)	0.18 (0.74)
	C7	8.35 (0.41)	12.44 (2.63)	−0.30 (3.04)	−1.2 (22.5)	1.14 (0.17)	0.61 (0.06)	0.49 (0.15)	−2.8 (17.0)	−0.20 (2.24)	0.5 (1.1)	0.08 (0.17)
	Mean	8.87 (1.02)	11.81 (2.37)	0.86 (1.55)	7.5 (13.4)	1.08 (0.27)	0.57 (0.14)	0.51 (0.12)	0.5 (16.0)	0.15 (1.87)	0.4 (4.5)	0.04 (0.53)
Inferior	C3	9.62 (1.47)	11.84 (1.86)	0.86 (1.31)	6.6 (9.6)	0.99 (0.21)	0.49 (0.10)	0.57 (0.13)	6.7 (13.8)	0.77 (1.84)	−0.9 (5.2)	−0.10 (0.62)
	C4	9.67 (0.89)	11.60 (2.10)	0.47 (1.21)	3.9 (9.8)	1.05 (0.25)	0.55 (0.13)	0.50 (0.07)	−1.0 (11.5)	−0.07 (1.50)	0.3 (9.8)	0.04 (1.01)
	C5	9.42 (1.02)	12.28 (1.79)	1.27 (2.05)	8.5 (19.3)	1.14 (0.24)	0.58 (0.10)	0.55 (0.13)	−9.0 (23.0)	−1.22 (2.41)	−1.7 (2.3)	−0.22 (0.30)
	C6	9.24 (1.00)	12.33 (1.32)	0.67 (1.41)	5.2 (12.2)	0.94 (0.23)	0.50 (0.10)	0.47 (0.11)	−3.1 (24.2)	−0.58 (2.89)	−1.9 (5.1)	−0.26 (0.61)
	C7	9.77 (1.01)	11.55 (1.69)	−1.29 (2.71)	−11.1 (21.2)	0.89 (0.09)	0.50 (0.05)	0.36 (0.10)	−6.8 (29.9)	−0.52 (3.10)	7.5 (10.9)	0.75 (1.01)
	Mean	9.52 (1.08)	11.96 (1.76)	0.65 (1.70)	4.7 (14.3)	1.02 (0.23)	0.53 (0.11)	0.51 (0.12)	−2.0 (19.7)	−0.28 (2.28)	−0.3 (6.8)	−0.06 (0.73)
P-value		**0.011*	0.489	0.135	0.070	0.116	0.081	0.379	0.278	0.236	0.467	0.488

P-values compare inferior and superior facets.

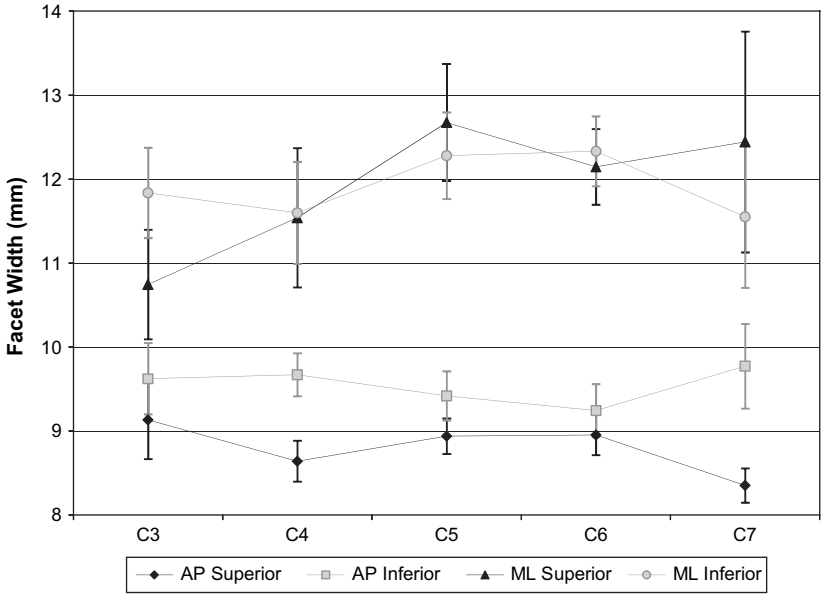

Fig. 5. Facet widths by level (mean ± standard error).

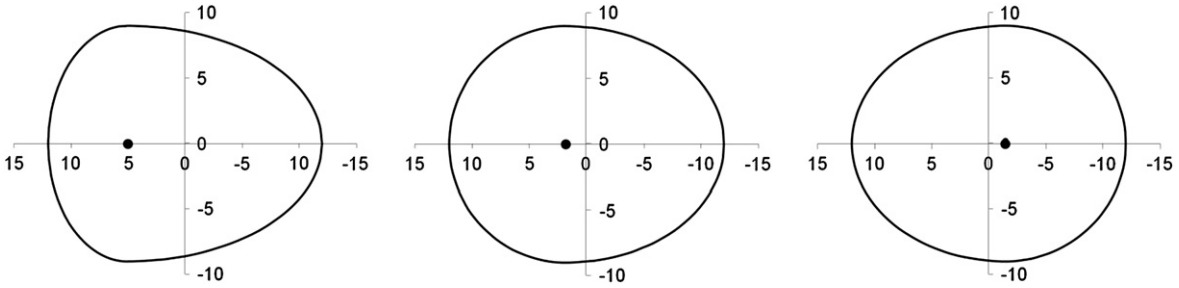

Fig. 6. Perimeter shapes for facets with ML (abscissa) and AP (ordinate) widths of 12 mm and 9 mm, respectively, showing the range of lateral shifts δ_L for the superior facets (mean ± 1 standard deviation). Lateral shifts of 21%, 8% (average shape), and −6% are depicted (left to right). Lateral edge is on the left.

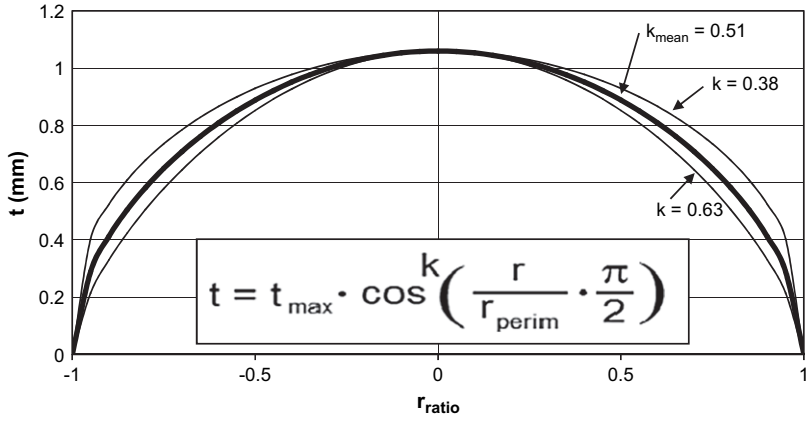

Fig. 7. Range of thickness distributions due to variation in the value of k (mean ± 1 standard deviation), when $t_{max} = 1.06$ mm. Reduced values for k represent flatter thickness distributions.

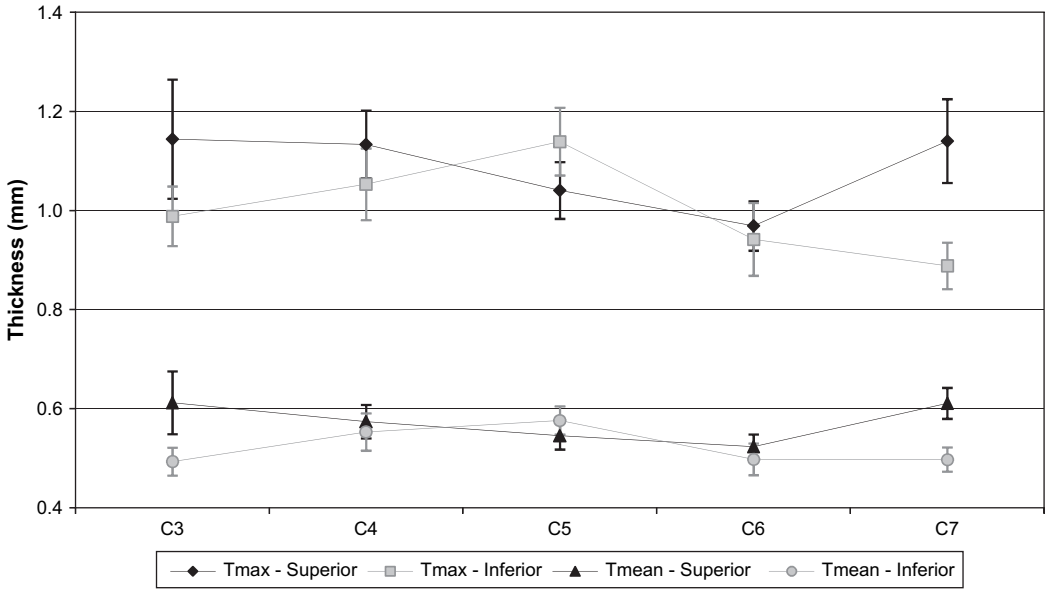

Fig. 8. Mean and peak facet cartilage thicknesses by level, with standard error.

($P = 0.012$) (Table I, Fig. 5). At the C3–C6 levels, the location of maximum AP width (δ_L) was shifted somewhat laterally, whereas medial shifts were observed at C7 (Table I, Fig. 6).

The range of thickness distribution shapes represented by the observed values of k is shown in Fig. 7. No significant differences in maximum or mean thickness were observed between the superior and inferior facets overall, and the only individual level exhibiting significant differences was C7 ($P = 0.03$ on maximum thickness) (Fig. 8). No significant differences in fit parameter k were observed overall (Fig. 9), and the modest decreasing trend as one moves caudally represents a slight flattening of the thickness profiles. High correlation (mean $r^2 = 0.97$) was also observed between the measured and fitted thickness distributions (indicating that the thickness fitting function used is able to accurately represent the range of cartilage thickness distributions observed).

No significant trends were observed in the ML and AP shifts of the location of maximum thickness relative to the geometric centers of the facets (Table I), and significant variability was observed in the location of maximum

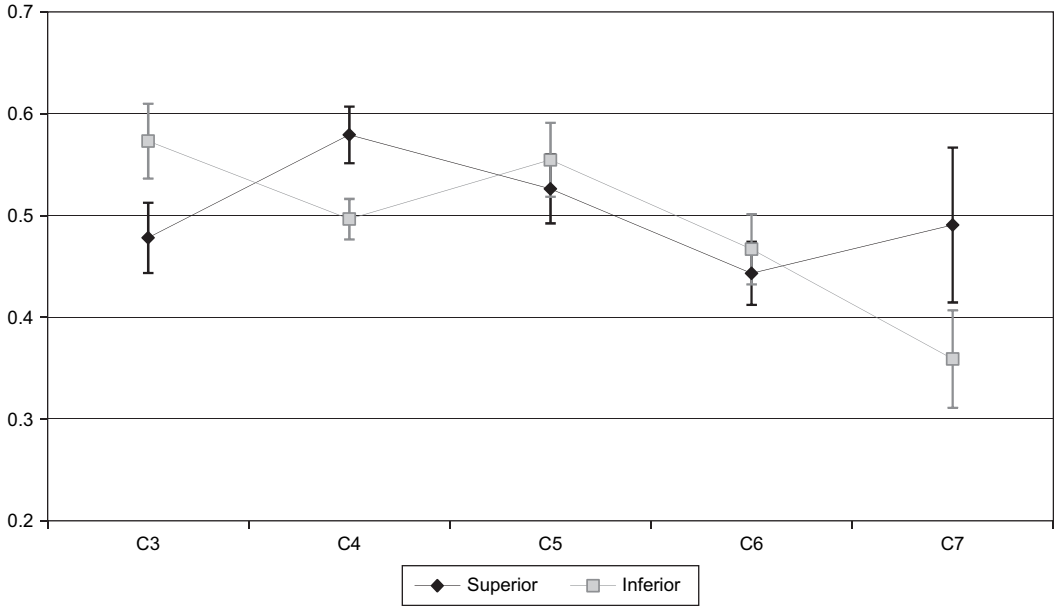

Fig. 9. Thickness distribution fit parameter k, with standard error. No significant differences were observed between inferior and superior facets overall, although differences were observed at the C3 and C4 levels ($P = 0.04$ and $P = 0.05$, respectively).

thickness. More variation was observed in the ML direction than in the AP direction (Table I), which confirms the gross experimental observation of thickness variability between subsequent slices.

Discussion

AP facet widths observed fall within the range reported by previous researchers, but the gap between the cartilaginous boundary and the perimeter of the bony geometry of the facet reported by Yoganandan *et al.* was not found to be present on all facets[6]. Some facets exhibited a prominent gap, while others exhibited full coverage. Additionally, it was observed that the gap varied in size and presence between subsequent slices on individual facets. Facet cartilage gap was generally maximized in the midsagittal slice, decreasing or disappearing both medially and laterally.

The shape of the facet cartilage thickness distributions observed is in good agreement with the average midsagittal profile given by Yoganandan, using the mean observed value of the fit parameter $k = 0.5$; i.e., this work represents a three-dimensional generalization of the midsagittal case.

While the facet cartilage is generally difficult to accurately identify using radiographic methods such as qCT, the underlying osteochondral interface is generally discernable. Three-dimensional surface reconstructions based on bony geometry frequently yield a readily identifiable facet region due to the curvature of the osteochondral interface of the facets. It is anticipated that utilization of a more physiologic cartilage thickness distribution in FE models will result in greater predictive accuracy with respect to cervical spine kinematics internal mechanical parameters. The consistency observed in the thickness distribution function in this study indicates that such a representation can be generated relatively easily, using the thickness distribution function reported here and the maximum thickness from either direct measurement or literature. While limitations of this study include a limited number of cadavers and the presence of degeneration on excluded levels, the independence of the maximum cartilage thickness and the shape factor k indicate that the model may be used to represent both full and reduced thickness cartilage distributions.

It was observed that the osteochondral interfaces of the inferior facets were more concave in the sagittal plane than those of the superior facets, with the result that the inferior articulating surfaces were slightly concave, whereas the superior articulating surfaces tended to be slightly convex. The congruence of these mating surfaces is therefore a function of both the shapes of the osteochondral surfaces and the thickness distributions of the cartilage on both facets. As stated above, it is expected that facet contact pressures and their distribution, and to a lesser degree spine kinematics, will be affected by the geometry and thickness distribution of the facet cartilage. Because the facet cartilage is neither flat nor a constant thickness, it is expected that oversimplification of these geometric properties in some currently published FE models most likely results in mechanical parameter prediction artifact. Computational models of the lower cervical spine that fail to account for these factors will therefore be limited in their ability to accurately predict pressures, stresses, and strains in the zygophyseal joints.

Conflict of interest

The authors claim no conflict of interest.

Acknowledgements

The authors would like to thank Dr A.S. Turner for providing the ovine and bovine specimens. Institutional research support provided by Synthes, Inc.

References

1. Battie MC, Videman T. Lumbar disc degeneration: epidemiology and genetics. J Bone Joint Surg Am 2006;88:3–9.
2. Crawford NR, Duggal N, Chamberlain RH, Chan PS, Sonntag VHK, Dickman CA. Unilateral cervical facet dislocation: injury mechanism and biomechanical consequences. Spine 2002;27:1858–64.
3. Onan OA, Hipp JA, Heggeness MH. Use of computed tomography image processing for mapping of human cervical facet surface geometry. Med Eng Phys 1998;20:77–81.
4. Panjabi MM, Duranceau J, Goel V, Oxland T, Takata K. Cervical human vertebrae – quantitative three-dimensional anatomy of the middle and lower regions. Spine 1991;16:861–9.
5. Panjabi MM, Oxland T, Takata K, Goel V, Duranceau J, Kraq M. Articular facets of the human spine – quantitative three-dimensional anatomy. Spine 1993;18:1298–310.
6. Yoganandan N, Knowles SA, Maiman DJ, Pintar FA. Anatomic study of the morphology of human cervical facet joint. Spine 2003;28(20):2317–23.